Pergamon

Cement and Concrete Research 32 (2002) 481–490

CEMENT AND CONCRETE RESEARCH

Water–cement ratio gradients in mortars and corresponding effective elastic properties

J.C. Nadeau*

Department of Civil and Environmental Engineering, Duke University, Box 90287, Durham, NC 27708-0287, USA

Received 21 June 2001; accepted 16 October 2001

Abstract

Water–cement ratio gradients are modeled through the interfacial transition zone (ITZ) of a mortar with spherical inclusions. The model is a function of the over-all water–cement ratio, volume fraction and radius of sand, specific gravity of cement and thickness of ITZ. Based on experimental data from the literature, the dependence of saturated, homogeneous cement paste is modeled as a function of water–cement ratio. Subsequently, the effective bulk and shear moduli for mortars are determined using a generalized self-consistent method. Finally, application of the model to data in the literature pertaining to elastic wave speeds in saturated mortars composed of 20–30 screened sand with an overall water–cement ratio of 0.3 yielded a mean ITZ thickness of 48.3 μm.

Keywords: Interfacial transition zone; Elastic moduli; Micromechanics; Modeling; Mortar

1. Introduction

The interfacial transition zone (ITZ) is characterized by gradients in porosity and chemistry which then affect the properties of cementitious composites. The ITZ arises due to a limitation in the packing of cement particles in the vicinity of the surface of aggregates [1] often referred to as the "wall effect." Scrivener and collaborators have observed an interfacial zone of 30–50 μm thick [2,p.154] in normal concretes by means of image analysis of SEM micrographs. Furthermore, the thickness appears to be independent of the size of the aggregate, however, it does appear to be a function of the size of largest cement particles, and to a lesser degree of the roughness of the aggregates, and the overall water–cement ratio [3].

Nilsen and Monteiro [4] concluded that the ITZ in mortars and concretes must be included in models pertaining to the effective elastic properties of such materials. The basis of their conclusion stemmed from the observation that measured elastic properties for mortars and concretes fall below the lower Hashin-Shtrikman bound computed assuming that concrete is a two-phase (aggregate and homogeneous cement paste) composite. There have been numerous subsequent investigations into the influence of the ITZ on the effective elastic properties of cementitious composites. Yang [5], Ramesh et al. [6] and Li et al. [7,8] have developed elastic models which approximate the entire ITZ as a single phase with homogeneous properties. As reaffirmed in a recent review [9], the gradients of the elastic properties within the ITZ are important and they have been addressed as a power law variation by Lutz and Zimmerman [10] for the bulk modulus and a piecewise constant variation by Garboczi and Bentz [11]. Both investigations [10,11] are limited, however, to dilute suspensions of aggregates.

In Section 2, a model is developed for the spatial variation in the water–cement ratio through the ITZ. In addition, a generalized self-consistent model [12], applicable to nondilute concentrations of aggregates, is applied to calculate the effective elastic properties of a mortar. In Section 3, a model for the dependence of the elastic properties of cement paste on water–cement ratio is constructed based on experimental data from the literature. In this paper, it is assumed that the length scale of the cement paste's microstructure is sufficiently small with respect to the size of the aggregate inclusions that it may be accurately modeled as homogeneous. The model is applied in Section

* Tel.: +1-919-660-5216; fax: +1-919-660-5219.
E-mail address: nadeau@duke.edu (J.C. Nadeau).

0008-8846/02/$ – see front matter
PII: S0008-8846(01)00710-4

4 to published data on wave speeds in saturated mortars to measure the thickness of the ITZ. Concluding remarks are presented in Section 5.

2. Model development

In this paper c will be used to denote volume fractions relative to the entire volume of the cementitious composite V while α will be used to denote local volume fractions. Thus, for example (Eq. (1)),

$$c_a = \frac{1}{V}\int_V \alpha_a dV \tag{1}$$

where the subscript a denotes "aggregate."

The distribution in the percentage area of anhydrous cement as a function of the distance from the surface of the aggregate x initially after mixing has been computed by Scrivener and Pratt [3, Fig. 1.5] using microstructural gradients measured in hardened pastes. In this case, because the results are presented for the state immediately after mixing, there are assumed to be no hydration products and thus the percent area of unhydrous cement is equal to the percent area of cement. It follows with appropriate care [13] that area fractions are equivalent to volume fractions. Thus, the initial percentage area distribution of anhydrous cement calculated by Scrivener and Pratt can be transformed to the volume fraction distribution of cement through the ITZ presented in Fig. 1. These data are fitted, by means of a least squares analysis, with the function:

$$\alpha_c(x) = \begin{cases} \bar{\alpha}_c^p\left[1 + a_c\left(\frac{x-\delta^p}{\delta^p}\right)^2\right] & 0 \le x \le \delta^p \\ \bar{\alpha}_c^p & x \ge \delta^p \end{cases} \tag{2}$$

where, a_c, $\bar{\alpha}_c^p$ and δ^p are fitting parameters. The parameter δ^p can be interpreted as the thickness of the ITZ, and $\bar{\alpha}_c^p$ as the local volume fraction of cement in the bulk paste. By bulk paste, it is meant the non-ITZ cement paste. A least squares analysis yields $a_c = -0.4959$, $\bar{\alpha}_c^p = 0.4430$ and $\delta^p = 21.52$ μm. The curve fit is presented in Fig. 1.

The local cement volume fraction through an ITZ of thickness δ is taken to vary in the following manner

$$\alpha_c(r) = \begin{cases} \bar{\alpha}_c\left[1 + a_c\left(\frac{r-r_a-\delta}{\delta}\right)^2\right] & r_a \le r \le r_a + \delta \\ \bar{\alpha}_c & r \ge r_a + \delta \end{cases} \tag{3}$$

where r is the distance from the center of an aggregate of radius r_a and $\bar{\alpha}_c$ is the local volume fraction of cement throughout the bulk paste. For lack of data, it is assumed that a_c is independent of all variables, thus,

$$a_c = -0.4959 \tag{4}$$

from the analysis associated with Eq. (2). This quantity $\bar{\alpha}_c$ is as yet unknown, but it will be derived below. This

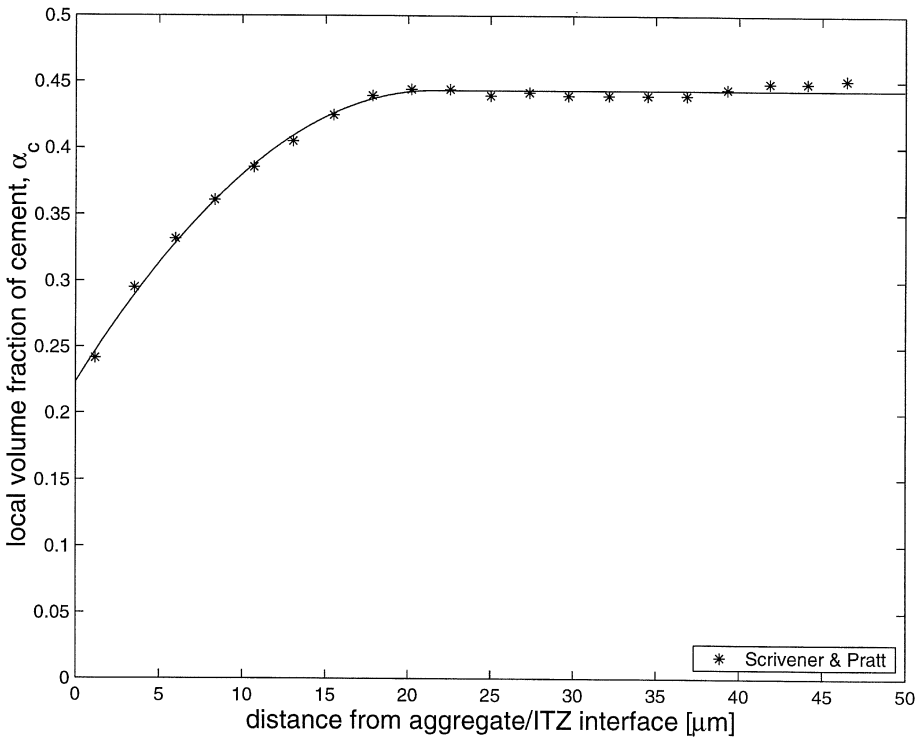

Fig. 1. Initial volume fraction of cement versus distance from aggregate interface. The solid line is the least squares fit of Eq. (2) to the data of Scrivener and Pratt.

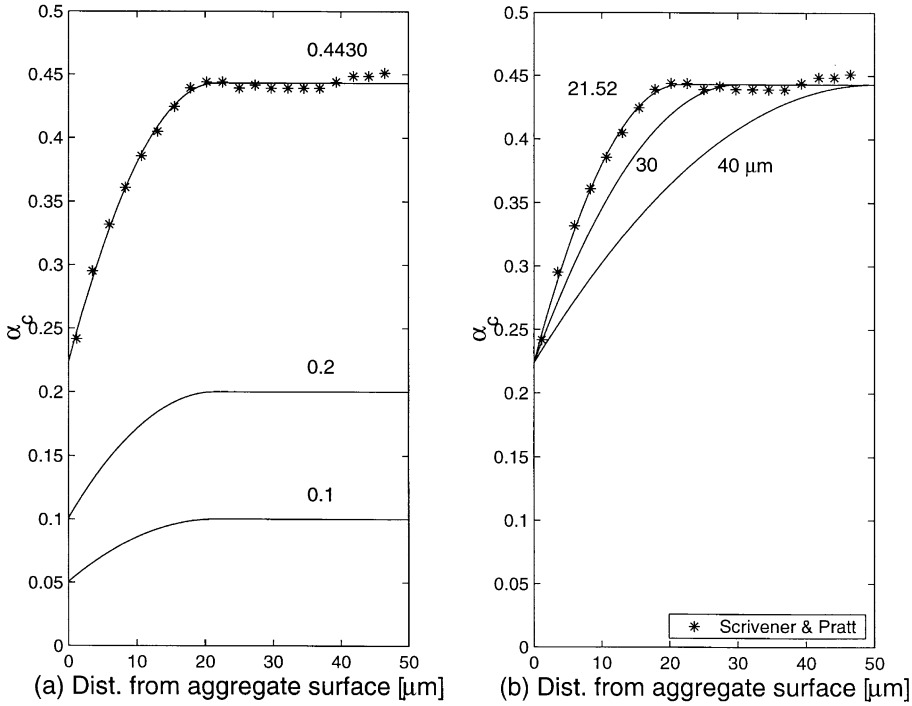

Fig. 2. Effect of variation in (a) $\bar{\alpha}_c$ and (b) δ on the distribution of cement through the ITZ.

assumption (3)–(4) recovers the finding of Scrivener and Pratt, by construction, and is consistent in that (Eq. (5))

$$\lim_{\alpha_c \to 0} \alpha_c = 0 \quad \forall r \geq r_a. \tag{5}$$

For illustrative purposes, and irrespective of keeping any other quantity such as bulk water–cement ratio constant, Eq. (3) is plotted varying $\bar{\alpha}_c$ and δ independently. Fig. 2(a) plots α_c with $\delta = 21.52$ for $\bar{\alpha}_c = 0.4430$, 0.2 and 0.1. Fig. 2(b) plots α_c with $\bar{\alpha}_c = 0.4430$ for $\delta = 21.52$, 30 and 40 μm. The data of Fig. 1 are also presented.

It now remains to calculate $\bar{\alpha}_c$ based upon the characteristic of the composite. For the present case, we shall assume a volume fraction c_a of equally sized spherical particles of radius r_a embedded within a cementitious matrix with an overall water–cement ratio w_o. For a volume V of composite the number of aggregate particles n_a contained within V is the volume of aggregates divided by the volume of a single aggregate particle:

$$n_a = \frac{c_a V}{\frac{4}{3}\pi r_a^3}. \tag{6}$$

The specific gravity of the cement is denoted by G_c. It is then possible to calculate the total volume of cement $V_c = c_c V$ as

$$V_c = \frac{1 - c_a}{1 + w_o G_c} V. \tag{7}$$

V_c will subsequently be decomposed into portions, within the ITZ, V_c^{ITZ} and outside the ITZ, i.e., the bulk paste, V_c^{nonITZ}. In other words, $V_c = V_c^{ITZ} + V_c^{nonITZ}$.

Consider a volume V of the spherically reinforced cementitious composite. Integrating Eq. (3) from $r = r_a$ to $r_a + \delta$ yields the volume of cement within a single ITZ. Multiplying this integral by the number of ITZs, i.e., Eq. (6), yields

$$V_c^{ITZ} = \frac{3 c_a \bar{\alpha}_c V}{r_a^3} \int_{r_a}^{r_a+\delta} \left[1 + a_c \left(\frac{r - r_a - \delta}{\delta} \right)^2 \right] r^2 \mathrm{d}r \tag{8}$$

which is the volume of cement located within all of the ITZs. Recalling that $\bar{\alpha}_c$ is the local volume fraction of cement in the bulk paste, the volume of non-ITZ cement in V is

$$\begin{aligned} V_c^{nonITZ} &= \bar{\alpha}_c [V - (V_a + V^{ITZ})] \\ &= \bar{\alpha}_c \left[V - \frac{4}{3} n_a \pi (r_a + \delta)^3 \right]. \end{aligned} \tag{9}$$

Substituting Eq. (6) into Eq. (9) and adding the result to Eq. (8) yields the total volume of cement in V, i.e., V_c. Equating this result to Eq. (7) and solving for $\bar{\alpha}_c$ yields

$$\bar{\alpha}_c = \frac{10(1 - c_a)}{(1 + w_o G_c) \left[a_c c_a \frac{\delta}{r_a} \left\{ \left(\frac{\delta}{r_a} \right)^2 + 5 \left(\frac{\delta}{r_a} \right) + 10 \right\} + 10(1 - c_a) \right]}. \tag{10}$$

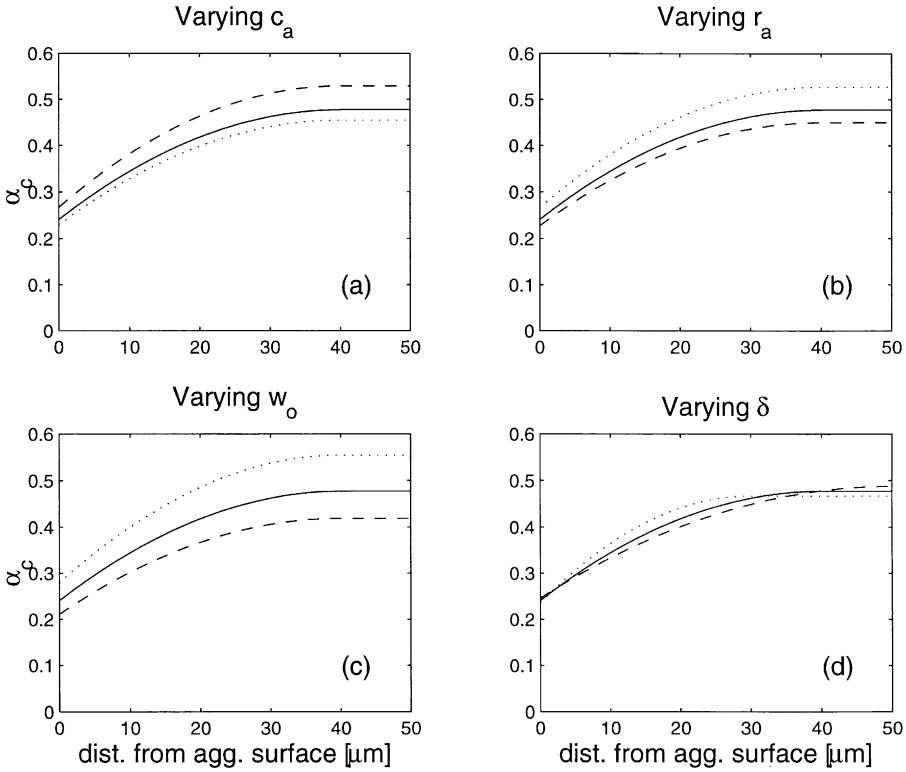

Fig. 3. Spatial variation of the local volume fraction of cement α_c through the ITZ into the bulk paste. The solid lines all correspond to (c_a, r_a, w_o, δ) = (0.4, 200, 0.4, 40 μm). The subfigures (a), (b), (c) and (d) depict the changes in α_c due to variations in c_a, r_a, w_o and δ, respectively. The dashed lines correspond to increasing the value of the quantity being varied relative to the solid line while the dotted line corresponds to decreasing the quantity in question; the specific values are detailed in Table 1.

Eq. (3), together with Eqs. (4) and (10), yields the spatial distribution of the volume of cement within the cement paste as a function of the volume fraction c_a and the radius r_a of aggregates, overall water–cement ratio w_o, thickness of the ITZ δ and the specific gravity of cement G_c. As such, the microstructure of the ITZ is a function of at least these parameters though the width of the ITZ is apparently a dependent variable and influenced by, for example, the size of cement particles as stated in Section 1. Because equal-sized aggregates are implicit in the derivation there are inherent limits on r_a, c_a and δ so that the ITZs of the neighboring aggregates do not overlap, a situation, which this theory does not explicitly admit. To ascertain these limits we consider the packing factor p, the volume of spheres in a unit volume (Eq. (11)):

$$p = c_a\left(1+\frac{\delta}{r_a}\right)^3. \tag{11}$$

For a given packing factor p there are imposed limits on r_a, c_a and δ (Eqs. (12)–(14)):

$$r_a^{min} = \frac{\delta}{\sqrt[3]{p/c_a}-1} \tag{12}$$

$$c_a^{max} = \frac{p}{(1+\delta/r_a)^3} \tag{13}$$

$$\delta^{max} = \left(\sqrt[3]{p/c_a}-1\right)r_a. \tag{14}$$

For FCC packing or an ideal HCP, the packing factor is $p = \pi\sqrt{2}/6 \doteq 0.740$.

For illustrative purposes, the radial variation of the volume of cement is presented in Fig. 3, while varying (c_a, r_a, w_o, δ) with $G_c = 3.15$. Table 1 provides a detailed legend.

The water–cement ratio w through the cement paste can be computed given the local volume fractions of other constituents. In this analysis, we shall assume that water is the only other constituent. Thus, for example, the cement paste is assumed not to have any macroscopic air voids. Local porosity, however, in the hydrated cement paste is of such a scale that it is incorporated in the elastic properties of the cement paste which vary as a function of the water–cement ratio. The local volume fraction of water is thus $\alpha_w = 1-\alpha_c$ and the water cement ratio is thus (Eq. (15)):

$$w = \frac{1-\alpha_c}{G_c\alpha_c}. \tag{15}$$

Table 1
Columns (1)–(6) provide the detailed legends for Figs. 3, 4, 8 and 9. $G_c = 3.15$. Columns (7)–(10) provide the mortar's effective moduli (using $\kappa_a = 44$ GPa, $\mu_a = 37$ GPa) while, for comparison, Columns (11) and (12) provide the mortar's effective properties assuming no ITZ, i.e., $\delta = 0$.

Plot legends											
Subplot (1)	Line type (2)	c_a (3)	r_a [μm] (4)	w_o (5)	δ [μm] (6)	κ* [GPa] (7)	μ* [GPa] (8)	E^* [GPa] (9)	ν^* (10)	$\kappa_{no\ ITZ}^*$ [GPa] (11)	$\mu_{no\ ITZ}^*$ [GPa] (12)
(a)	dashed	0.6	200	0.4	40	27.52	17.75	43.82	0.235	30.58	20.43
	solid	0.4	200	0.4	40	23.30	13.52	33.99	0.257	26.00	15.67
	dotted	0.2	200	0.4	40	20.94	11.15	28.41	0.274	22.30	12.13
(b)	dashed	0.4	800	0.4	40	25.05	14.75	37.00	0.254	26.00	15.67
	solid	0.4	200	0.4	40	23.30	13.52	33.99	0.257	26.00	15.67
	dotted	0.4	100	0.4	40	22.83	13.31	33.43	0.256	26.00	15.67
(c)	dashed	0.4	200	0.5	40	18.71	10.15	25.78	0.270	21.08	12.32
	solid	0.4	200	0.4	40	23.30	13.52	33.99	0.257	26.00	15.67
	dotted	0.4	200	0.3	40	27.18	16.50	41.16	0.248	29.54	18.50
(d)	dashed	0.4	200	0.4	50	23.00	13.34	33.54	0.257	26.00	15.67
	solid	0.4	200	0.4	40	23.30	13.52	33.99	0.257	26.00	15.67
	dotted	0.4	200	0.4	30	23.73	13.79	34.66	0.257	26.00	15.67

For illustrative purposes, the radial distribution of the water–cement ratio, for the cases considered in Fig. 3, are plotted in Fig. 4. Note that for the solid lines, with an overall water–cement ratio $w_o = 0.4$, the bulk paste water–cement ratio is lower at 0.34 and the water–cement ratio at the aggregate surface is higher at 1.01.

Let $\kappa_p(w)$ and $\mu_p(w)$ denote the elastic properties of the cement paste as a function of the water–cement ratio. These expressions will be modeled explicitly in Section 3 for saturated cement pastes. It is assumed that the elastic properties of the homogeneous cement paste specimens are representative of the local elastic properties of the

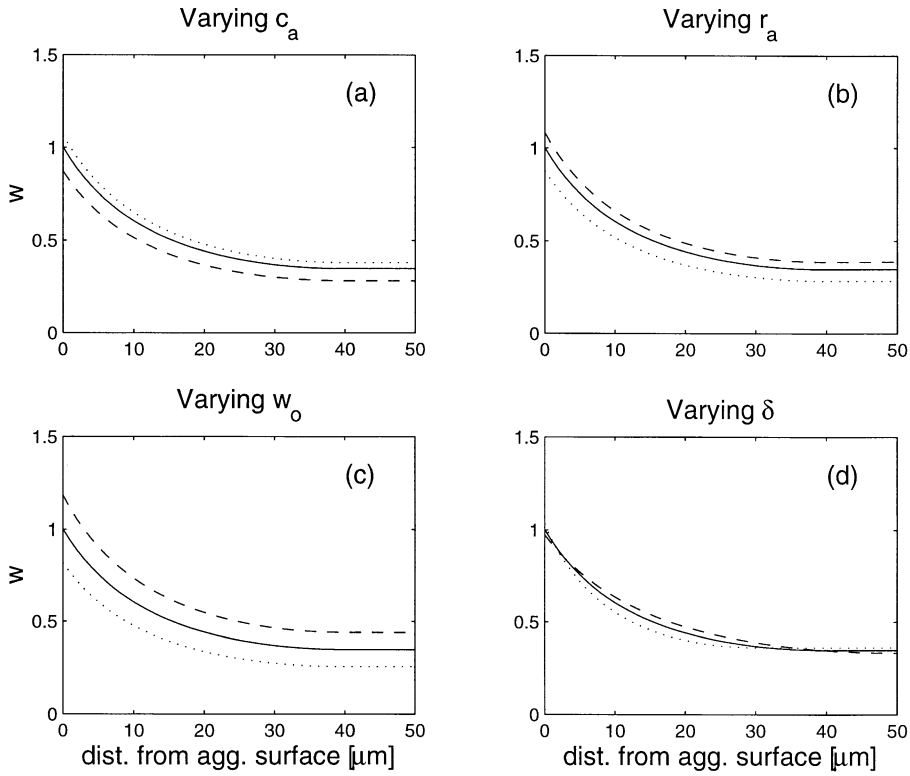

Fig. 4. Spatial variation of w through the ITZ into the bulk paste. The solid lines all correspond to (c_a, r_a, w_o, δ) = (0.4, 200, 0.4, 40 μm). The subfigures (a), (b), (c) and (d) depict the changes in w due to variations in c_a, r_a, w_o and δ, respectively. The dashed lines correspond to increasing the value of the quantity being varied relative to the solid line while the dotted line corresponds to decreasing the quantity in question; the specific values are detailed in Table 1.

cement paste within the ITZ. As such, it is inherently assumed that the elastic properties within the ITZ are isotropic. The validity of this assumption should be investigated as calcium hydroxide if preferentially oriented within the ITZ (with the *c*-axis parallel to the aggregate surface) [2,p.151] and thus may be indicative of anisotropic properties within the ITZ. At the scale of the ITZ (approximately 50-μm thick) the scale of the microstructure is not much smaller than this dimension and the gradients across this distance are quite large. The application of pointwise homogenization, such as what is inherently occuring here, has been documented by Reiter et al. [14] and Dolbow and Nadeau [15] to be plausible through the investigation of numerical studies. Substituting Eq. (15) into κ_p and μ_p thus yields the variation in elastic properties through the ITZ and into the bulk paste. The elastic properties of the bulk paste will be denoted κ_{bp} and μ_{bp}.

The effective elastic bulk κ^* and shear μ^* moduli of the composite will be evaluated using the $(n+1)$-phase spherical model [12]. This is a generalized self-consistent model and it recovers the effective shear modulus prediction of the three-phase model developed by Christensen and Lo [16] for biconstituent, particulate reinforced composites. In order to apply the $(n+1)$-phase model to the current application the thickness of the ITZ is divided into k equally sized divisions. (Calculations performed herein utilize $k=50$.) With the origin placed at the center of a spherical aggregate the radial variation in, for example, the bulk modulus is presented in Fig. 5. The $(n+1)$-model requires that the i-th phase has homogeneous properties, thus, for example the bulk modulus of the i-th phase (for $2 \le i \le k+1$) is taken as the average of the bulk moduli at $r=r_i$ and r_{i+1}. The moduli in phases 1, $k+2$, and $k+3$ are already homogeneous.

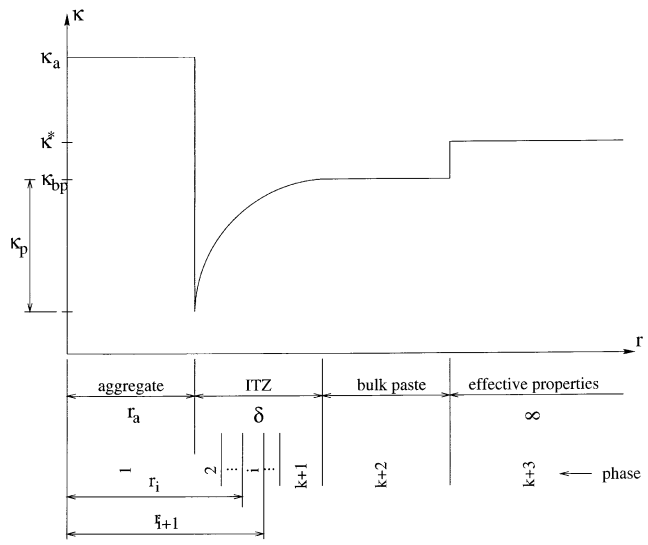

Fig. 5. Bulk modulus κ variation in the radial direction for the $(n+1)$-phase, generalized self-consistent model where r is measured from the center of the aggregate. A similar variation occurs with the shear modulus μ.

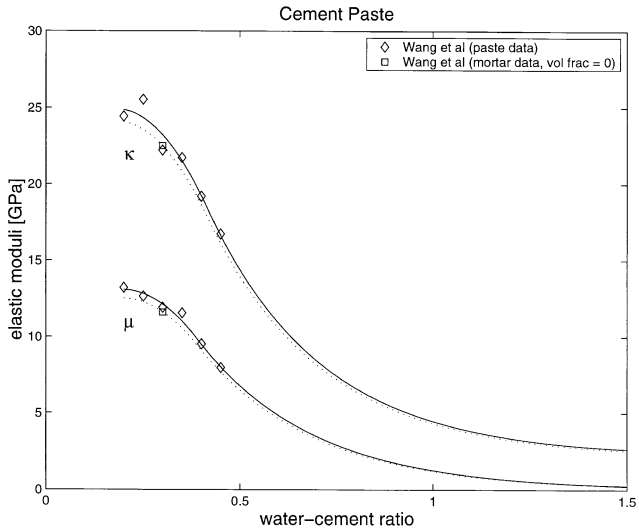

Fig. 6. Bulk κ and shear μ moduli for saturated cement paste versus water–cement ratio. The solid lines are the least squares fit of Eq. (17) to the respective (diamond) data for cement paste. The dotted curves are the respective solid curves scaled by a factor so as to pass through the respective squares data point which is taken from the mortar data with a volume fraction of zero, i.e., a cement paste. The dotted lines are subsequently assumed to model the water–cement ratio dependence of the cement paste in all of the Wang et al. mortar specimens.

3. Saturated cement paste

Wang et al. [17] measured the variation in the bulk and shear moduli, by way of elastic wave speeds, with respect to various overall water–cement ratios between the range 0.2 and 0.45 for cement pastes made from ASTM Type I/II Portland cement. After demolding the specimens were stored in lime-saturated water until testing thus we will term these pastes to be saturated. These data are presented as diamonds in Fig. 6. Given the limited range of water–cement ratios considered, and the necessity herein to quantify cement paste properties over a wide range of water–cement ratios (see Fig. 4), data [18] on the variation of Young's modulus E with respect to water–cement ratio over the range of 0.3–0.6 was also considered. These data are presented as circles in Fig. 7. The corresponding Young's moduli of Wang et al's data are also presented in Fig. 7, as diamonds. It is assumed that Simeonov et al's data (i.e., the circles) can be adequately, and appropriately, fitted with an exponential function of the form

$$E(w) = a_E \exp(b_E w) \tag{16}$$

where a_E and b_E are fitting parameters. Since the cement pastes are fully saturated, it has been assumed that as

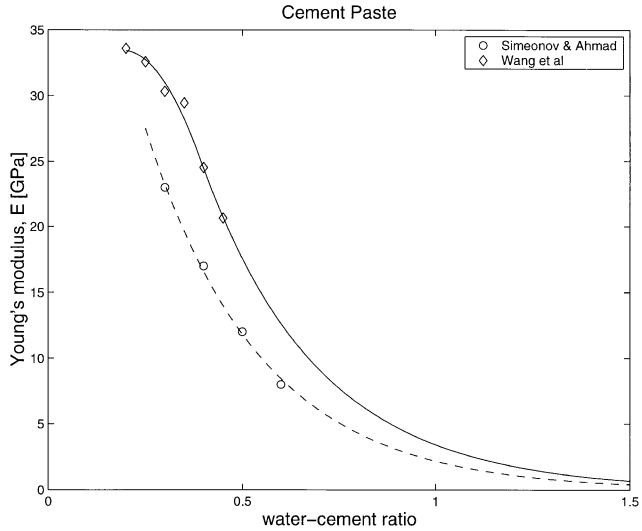

Fig. 7. Young's modulus E of cement paste versus water–cement ratio. The dashed curve is the least squares fit of Eq. (16) to the data of Simeonov and Ahmad. The solid curve and the diamonds represent the Young's moduli for the corresponding results presented in Fig. 6.

$w \to \infty$, Young's modulus E will tend to that of water, i.e., 0. A least squares analysis yielded $a_E = 63.9506$ GPa and $b_E = -3.3754$. This best fit is the dashed line in Fig. 7.

It is assumed that the functional dependence of the bulk and shear moduli on w for $w > 0.4$ is the same as that for the Young's modulus. In other words, it is assumed that $\kappa(w) = a_\kappa \exp(b_E w) + \kappa_{water}$ where $\kappa_{water} = 2.2$ GPa, b_E has been previously determined and a_κ is a fitting parameter. A similar equation can be constructed for the shear modulus where $\mu_{water} = 0.0$ GPa. For "intermediate" water–cement ratios (i.e., 0.2 to approximately 0.4) the data are not adequately modeled by an exponential function thus a second-order polynomials is used in this region which will intersect and be tangent to the exponential function at $w = \bar{w}$. In other words,

$$\kappa = \begin{cases} c_\kappa + d_\kappa w + e_\kappa w^2 & 0.2 \le w \le \overline{w}_\kappa \\ a_\kappa \exp(b_E w) + \kappa_{water} & w \ge \overline{w}_\kappa \end{cases} \tag{17}$$

where

$$d_\kappa = a_\kappa b_E \exp(b_E \overline{w}_\kappa) - 2 e_\kappa \overline{w}_\kappa \tag{18}$$

$$c_\kappa = a_\kappa \exp(b_E \overline{w}_\kappa) + \kappa_{water} - d_\kappa \overline{w}_\kappa - e_\kappa \overline{w}_\kappa^2. \tag{19}$$

Eqs. (18) and (19) were arrived at from the requirements that the two functions of Eq. (17) have the same value and slope at $w = \bar{w}_\kappa$. The variables α_κ, e_κ and $\bar{w}_\kappa$ are fitting parameters and, again, $b_E = -3.3754$ from the analysis on the Young's modulus data.

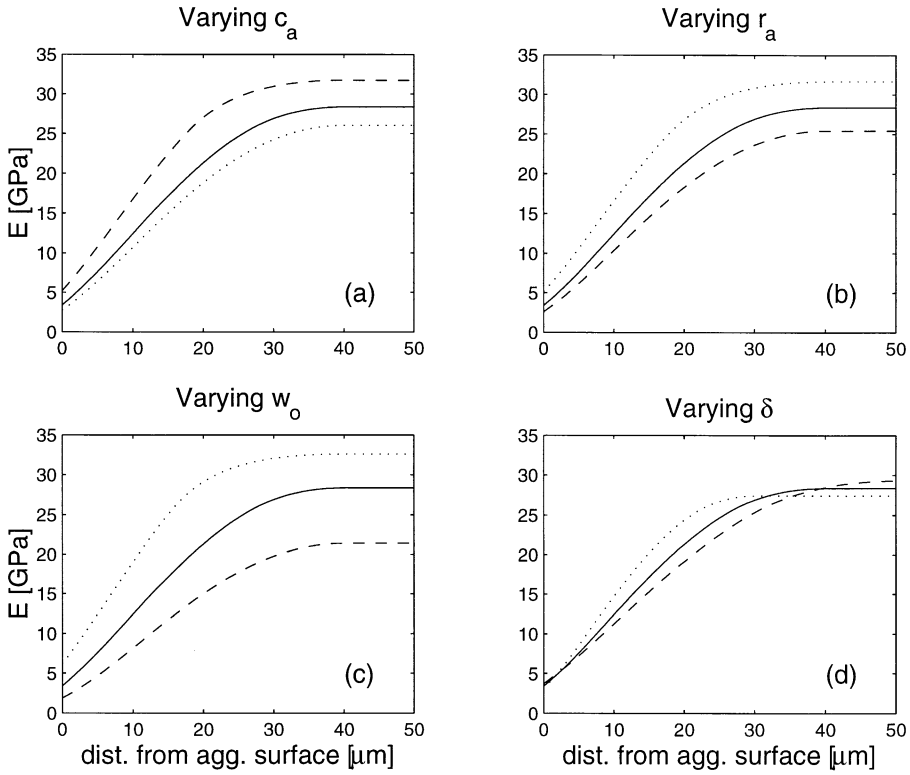

Fig. 8. Spatial variation of the cement paste's Young's modulus E through the ITZ into the bulk paste. The solid lines all correspond to (c_a, r_a, w_o, δ) = (0.4, 200, 0.4, 40 μm). The subfigures (a), (b), (c) and (d) depict the changes in E due to variations in c_a, r_a, w_o and δ, respectively. The dashed lines correspond to increasing the value of the quantity being varied relative to the solid line while the dotted line corresponds to decreasing the quantity in question; the specific values are detailed in Table 1.

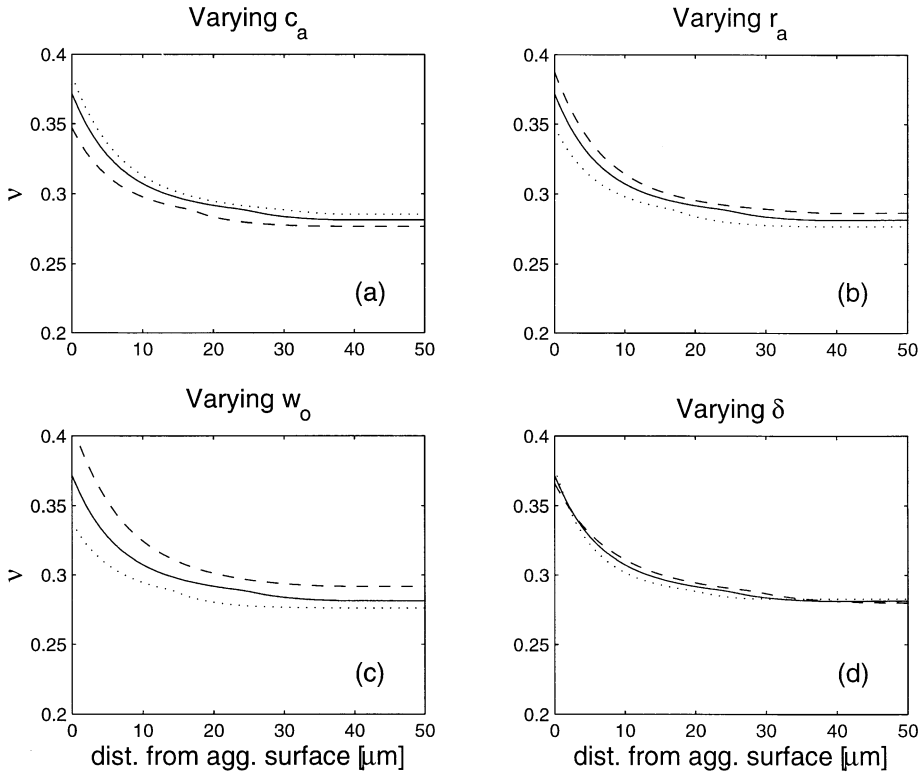

Fig. 9. Spatial variation of the cement paste's Poisson's ratio ν through the ITZ into the bulk paste. The solid lines all correspond to (c_a ,r_a, w_o, δ) = (0.4, 200, 0.4, 40 μm). The subfigures (a), (b), (c) and (d) depict the changes in ν due to variations in c_a, r_a, w_o and δ, respectively. The dashed lines correspond to increasing the value of the quantity being varied relative to the solid line while the dotted line corresponds to decreasing the quantity in question; the specific values are detailed in Table 1.

Using the bulk data for $w = 0.4$ and 0.45, a least squares analysis yielded $a_\kappa = 65.8999$ GPa. A subsequent least squares analysis using all of the bulk data yielded $e_\kappa = -117.3764$ GPa and $\bar{w}_\kappa = 0.4142$. The curve fit is illustrated in Fig. 6 as the solid line through the bulk data. A similar analysis (with an appropriate change in notation, namely, $\kappa \rightarrow \mu$) for the shear data yielded $a_\mu = 36.6103$ GPa, $e_\mu = -84.8249$ GPa and $\bar{w}_\mu = 0.3892$. This curve fit is illustrated in Fig. 6 as the solid line through the shear data. The Young's modulus consistent with the curve fits of the bulk and shear moduli is presented as the solid line in Fig. 7.

For illustrative purposes the radial distribution of the Young's modulus and Poisson's ratio, for the cases considered in Fig. 3, are plotted in Figs. 8 and 9, respectively. The results of Lutz et al. [19] indicate that the bulk modulus of the cement paste at the aggregate surface is a approximately 50–70% of the bulk paste value. From the results presented in Figs. 8 and 9 it is deduced that the bulk modulus at the aggregate interface is 20% of the bulk paste value, for the solid lines. The shear modulus at the interface is 12% of the bulk paste value. Also, note that for the saturated cement paste considered the Poisson's ratio ν in the paste is significantly larger at the aggregate surface than in the bulk cement paste.

Given the variation in the elastic moduli of saturated, homogeneous cement paste as a function of water–cement ratio, the homogenization technique outlined in Section 2 is applied to compute the effective elastic properties of the mortars that have been featured in Figs. 3, 4, 8 and 9. These effective properties are presented in columns (7) through (10) of Table 1. For comparison, the effective properties estimated by disregarding the ITZ and assuming that the saturated cement paste is homogeneous yields the results presented in columns (11) and (12). Note that, in general, the effective moduli incorporating the ITZ are approximately 10–20% less than the effective moduli that do not incorporate the ITZ. This finding is consistent with the hypothesis in the paper of Nilsen and Monteiro

Table 2
Elastic properties for sand (Kuster and Toksöz, 1974)

Elastic property	Value
Bulk modulus, κ	44 GPa
Shear modulus, μ	37 GPa
Young's modulus, E	88.7 GPa
Poisson's ratio, ν	0.172

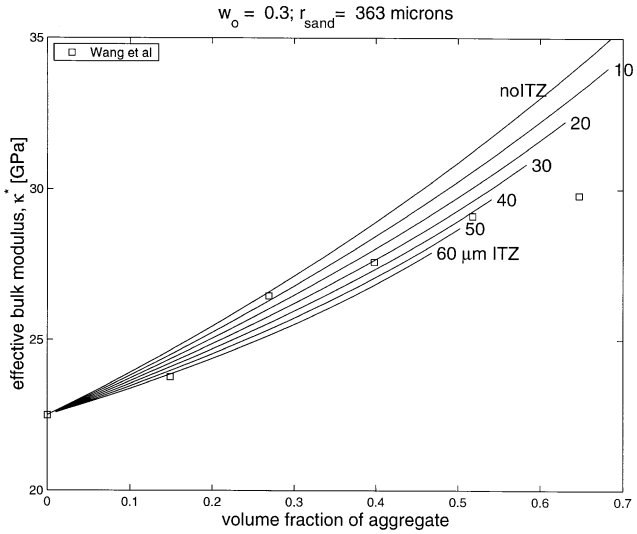

Fig. 10. Effective bulk modulus κ* versus aggregate volume fraction c_a for various thicknesses of ITZ δ. The solid line denoted "no ITZ" is the three-phase model, which does not incorporate the ITZ. The squares denote the experimental data of Wang et al.

[4] that surmised that a third phase, the ITZ, was causing the experimental data to violate the Hashin-Shtrikman lower bound.

4. Application of model

Predictions of the current model are compared with the elastic data [17] for saturated mortar specimens composed of ASTM Type I/II Portland cement and screened 20–30 Ottawa sand with $w_o = 0.3$ overall water–cement ratio.

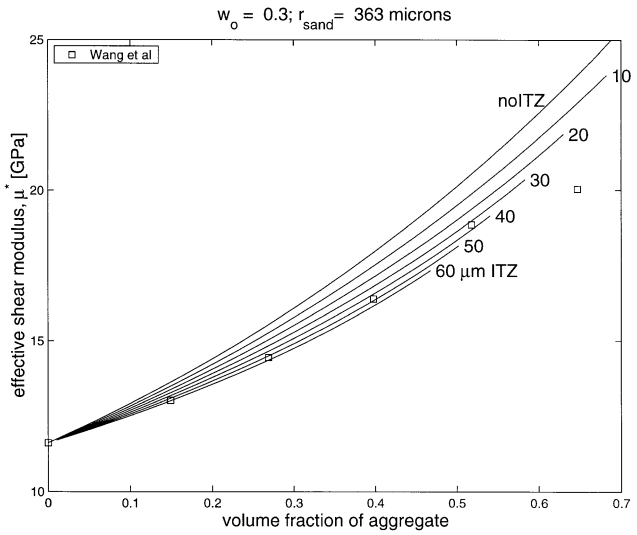

Fig. 11. Effective shear modulus μ* versus aggregate volume fraction c_a for various thicknesses of ITZ δ. The solid line denoted "no ITZ" is the three-phase model, which does not incorporate the ITZ. The squares denote the experimental data of Wang et al.

Table 3
Interpolated measurements of the thickness of the ITZ based on experimental measurements of Wang et al.

	Thickness of ITZ [μm]				
c_a	κ data	μ data		All data	Chauvenet criteria
0.15	67.2	58.2			
0.27	4.2	53.8			
0.40	31.9	47.6			
0.52	44.9	34.5			
			mean [μm]	42.8	48.3
			S.D. [μm]	19.5	12.6

Assuming a uniform distribution of aggregate sizes between the 600 and 850 μm sieve openings yields an average radius of $r_a = 363$ μm. The moduli of sand are taken as the typical values for a sandstone or quartz-rich rock adopted by Kuster and Toksöz [20]. These elastic properties are presented in Table 2. These moduli have been adopted by other researchers [19,21] for sand with success and will thus be used herein. However, it should be noted that, using single crystal quartz elastic coefficients [22,p.143] at 25°C, the self-consistent approximation to the polycrystalline properties can be calculated [23] yielding $\kappa^* = 36.5$ GPa and $\mu^* = 44.7$ GPa.

The measured mortar moduli [17] for 0% volume fraction of sand ($c_a = 0$), thus equivalent to the cement paste matrix moduli, are presented as squares in Fig. 6. Assuming these moduli to be representative of the cement paste matrix moduli for all of the mortar specimens, the curve fits (solid lines) in Fig. 6 are uniformly scaled to pass through the corresponding square data points. The scaled moduli are presented as dotted lines.

Figs. 10 and 11 present the effective bulk κ* and shear μ* moduli, respectively, for the mortar specimens considered by Wang et al. [17] for various values of the thickness of the ITZ, δ. The solid lines terminate when the limit of the theory (i.e., overlapping ITZs) is reached according to Eq. (13). The mortar data are depicted as squares. An interpolation/extrapolation of the results depicted in these plots yield the ITZ thicknesses tabulated in Table 3. Utilizing all eight data points the mean ITZ thickness is δ = 42.8 μm with a standard deviation of 19.5 μm. Chauvenet's criterion [24,p.73] identifies the 4.2-μm thickness measurement as suspect. Removing this data point yields a mean of δ = 48.3 μm with a standard deviation of 12.6 μm.

5. Closure

A model has been presented which quantifies the spatial distribution of cement and water–cement ratio gradient through the ITZ of cementitious composites. This model has for the time being assumed that the parameter a_c is constant and approximately equal to -0.5. Further investigations are required to ascertain any dependencies that this

parameter may have and perhaps if different functional forms of the variation of the cement content through the ITZ are warranted. Specific results were obtained for mortars with screened, spherical aggregates, however, results can be generalized to graded aggregates and extended to concretes; this work is underway. A model accounting for the effect of water–cement ratio on the elastic properties of a saturated Type I/II Portland cement paste was developed based on experimental data in the literature thus enabling the prediction of effective elastic properties through application of the generalized self-consistent, $(n+1)$-phase model. Based on the wave speed data of Wang et al. [17] on saturated mortars the proposed model "measures" the thickness of the ITZ to be $\delta = 48.3$ μm. The standard deviation of the measurements was 12.6 μm. It is significant to note that the developed model does not possess any "fitting" parameters to optimize the correlation to the experimental data of Wang et al.

The model predicts local water–cement ratios at aggregate interfaces as high as 3+times the bulk paste water–cement ratio (see Fig. 4) which, in turn, result in the bulk paste have a lower water–cement ratio than the overall water–cement ratio. Furthermore, the model indicates that cement-pastes within mortars are predicted to have elastic moduli at the aggregate surface which are 10–20% of the bulk paste properties (see Fig. 8).

It is believed that this investigation will advance efforts in designing cementitious composites [9] which will mitigate the detrimental effects that the ITZ has on the elastic properties. It has been demonstrated by Nadeau and Ferrari [25] that spatial gradients of microstructure can be significant even in comparison to significant variations in non-microstructural quantities [26] and this is by all observations the case in cementitious composites with ITZs.

Acknowledgments

The assistance of Chris Shoemaker is acknowledged as is his support through the Pratt School of Engineering's Engineering Undergraduate Fellows program administered by Martha Absher.

References

[1] E.J. Garboczi, D.P. Bentz, Digital simulation of the aggregate–cement paste interfacial zone in concrete, J. Mater. Res. 6 (1) (1991) 196–201.
[2] K. Scrivener, The microstructure of concrete, J. Skalny (Ed.), Materials Science of Concrete, vol. 1, American Ceramic Society, Westerville, OH, 1989, pp. 127–161.
[3] K. Scrivener, P. Pratt, Characterization of interfacial microstructure, RILEM Report 11, E&FN Spon, London, 1996, pp. 1–17 (Chap. 1).
[4] A.U. Nilsen, P.J.M. Monteiro, Concrete: A three-phase material, Cem. Concr. Res. 23 (1) (1993) 147–151.
[5] C.C. Yang, Effect of the transition zone on the elastic moduli of mortar, Cem. Concr. Res. 28 (5) (1998) 727–736.
[6] G. Ramesh, E.D. Sotelino, W.F. Chen, Effect of transition zone on elastic moduli of concrete materials, Cem. Concr. Res. 26 (4) (1996) 611–622.
[7] G. Li, Y. Zhao, S.-S. Pang, Y. Li, Effective Young's modulus estimation of concrete, Cem. Concr. Res. 29 (1999) 1455–1462.
[8] G. Li, Y. Zhao, S.-S. Pang, Four-phase sphere modelling of effective bulk modulus of concrete, Cem. Concr. Res. 29 (1999) 839–845.
[9] A. Bentur, M.G. Alexander, A review of the work of the RILEM TC 159-ETC: Engineering of the interfacial transition zone in cementitious composites, Mater. Struct. 33 (2000) 82–87.
[10] M. Lutz, R. Zimmerman, Effect of the interphase zone on the bulk modulus of a particulate composite, J. Appl. Mech. 63 (1996) 855–861.
[11] E. Garboczi, D. Bentz, Analytical formulas for the interfacial transition zone properties, Adv. Cem. Based Mater. 6 (1997) 99–108.
[12] E. Herve, A. Zaoui, n-layered inclusion-based micromechanical modelling, Int. J. Eng. Sci. 31 (1) (1993) 1–10.
[13] D.X. Shi, D. Winslow, Accuracy of a volume fraction measurement using areal image analysis, J. Testing Eval. 19 (3) (1991) 210–213.
[14] T. Reiter, G.J. Dvorak, V. Tvergaard, Micromechanical models for graded composite materials, J. Mech. Phys. Solids 45 (8) (1997) 1281–1302.
[15] J. Dolbow, J. Nadeau, On the use of effective properties for the fracture analysis of microstructured materials, Eng. Fracture Mech., in press.
[16] R.M. Christensen, K.H. Lo, Solutions for effective shear properties in three phase sphere and cylinder models, J. Mech. Phys. Solids 27 (4) (1979) 315–330 (erratum, 34(6):639).
[17] J. Wang, J. Lubliner, P. Monteiro, Effect of ice formation on the elastic moduli of cement paste and mortar, Cem. Concr. Res. 18 (1988) 874–885.
[18] P. Simeonov, S. Ahmad, Effect of transition zone on the elastic behavior of cement-based composites, Cem. Concr. Res. 25 (1) (1995) 165–176.
[19] M.P. Lutz, P.J.M. Monteiro, R.W. Zimmerman, Inhomogeneous interfacial transition zone model for the bulk modulus of mortar, Cem. Concr. Res. 27 (7) (1997) 1113–1122.
[20] G.T. Kuster, M.N. Toksöz, Velocity and attenuation of seismic waves in two-phase media: Part I. Theoretical formulations, Geophysics 39 (5) (1974) 587–606.
[21] R.W. Zimmerman, M.S. King, The effect of the extent of freezing on seismic velocities in unconsolidated permafrost, Geophysics 51 (6) (1986) 1285–1290.
[22] F. Birch, Compressibility; elastic constants, Handbook of Physical Constants, Geological Society of America, New York, 1966, pp. 97–173 (Chap. 7).
[23] J.C. Nadeau, M. Ferrari, On optimal zeroth-order bounds with application to Hashin-Shtrikman bounds and anisotropy parameters, Int. J. Solids Struct. 38 (2001) 7945–7965.
[24] J. Holman, Experimental Methods for Engineers, fourth ed., McGraw-Hill, New York, 1984.
[25] J.C. Nadeau, M. Ferrari, Microstructural optimization of a functionally graded transversely isotropic layer, Mech. Mater. 31 (10) (1999) 637–652.
[26] J.C. Nadeau, X.N. Meng, On the response sensitivity of an optimally designed functionally graded layer, Composites, Part B 31 (2000) 285–297.